US HL-LHC Accelerator Upgrade Project

Analysis of MQXFA13 Test Non-Conformity

Editors: G. Ambrosio, M. Baldini, P. Ferracin

G. Ambrosio, M. Baldini, A. Bartkowska, A. Ben Yahia, J. Blowers, D. Cheng, M. Crouvizier, J. Doyle, P. Ferracin, L. Garcia Fajardo, S. Izquierdo Bermudez, V. Marinozzi, A. Moros, M. Naus, K. Ray, J. Schmalzle, S. Sgobba, G. Vallone

TABLE OF CONTENTS

1. Introduction

MQXFA13 is the 6th MQXFA series magnet fabricated by AUP. Main data about components and assembly of this magnet can be found in the MQXFA13 Fabrication report [1].

MQXFA13 was able to reach and hold acceptance current during vertical test [2]. Nonetheless, it showed long training in a single coil (227) and it quenched in coil 227 at every up-ramp following a down-ramp at -100 A/s. This behavior triggered the concern of possible locale damage in coil 227 and that MQXFA may not meet acceptance requirements [3] during subsequent tests or operation.

Preliminary analysis of possible causes highlighted that the ends of MQXFA13 coils are among those with the smallest arc-length. The small arc-length of all coils in the lead end is expected to reduce friction with the structure allowing more strain at the transition between straight section and ends. This is the area where conductor damage was found in the limiting coils of MQXFA07 [4] and MQXFA08 [5]. The risk of damage to the other MQXFA13 coils suggested stopping the test for replacing coil 227 with a new coil.

This report presents the analysis of this issue and possible causes.

2. Test Results and Analysis

2.1. Quench History

MQXFA13 quench history plot is shown in Fig 2.1 and was presented at the MQXFA13, MQXFA8b and MQXFA14b Test Results Meeting [2].

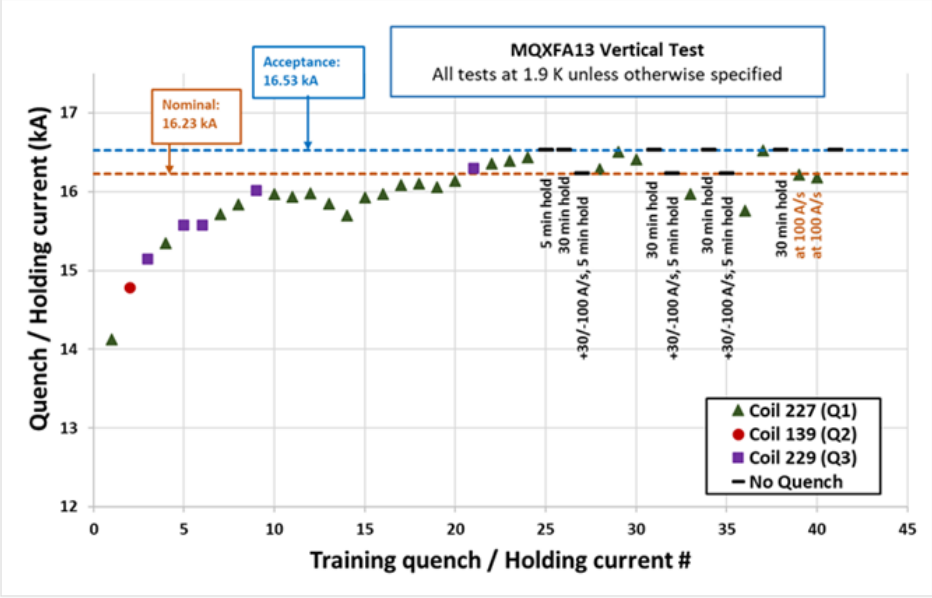

Figure 2.1: MQXFA13 training history

The main test results of MQXFA13 can be summarized as follows.

- Quench #10 (at 15969 A) had some unusual features: quench antenna signal 6 times larger than usual (Fig 2.2) and significantly faster voltage rise than all other quenches at similar current (Fig 2.3). It occurred in the lead end of coil 227 at 2.01 m from magnet center. After this quench MQXFA13 had 6 quenches at similar or lower current (as low as 15699 A). All of them in coil 227, and 5 of them in the same location of quench #10.

- Starting from quench #17 MQXFA13 resumed training, and was able to hold acceptance current at the end of ramp #25. In this phase of the training all quenches except one (#21) occurred in coil 227, and most of them within +/- 1 m from magnet center.
- After current ramp #27 (up at +30 A/s, down at -100 A/s) MQXFA13 quenched during ramp #28 (quench #25) at 16285 A. This quench started in coil 227 lead end at 2.01 m from magnet center.
- Subsequently, after 2 training quenches, MQXFA13 was able to hold again acceptance current.
- But after current ramp #32 (up at +30 A/s, down at -100 A/s) MQXFA13 quenched during ramp #33 (quench #28) at 15968 A. Also this quench was in coil 227 lead end at 2.01 m from the magnet center. This was the second quench in the current ramp following a ramp down from nominal at -100 A/s.
- The same behavior occurred after ramp #35 (up at +30 A/s, down at -100 A/s). MQXFA13 quenched during ramp #36 (quench #29) at 15759 A. Also this quench was in coil 227 lead end at 2.01 m from the magnet center.
- In ramp #38 MQFXA13 was still able to hold acceptance current for 30 minutes.
- Ramps #39 and #40 were performed at 100 A/s and MQXFA13 quenched in coil 227 in both of ramps at 16221 A (in the lead end at 2.01 m from magnet center) and at 16185 A (in the retrun end at -1.99 m from the magnet center).
- In the last ramp (#41) MQXFA13 was again able to hold acceptance current for 30 minutes.

MQXFA13 did not have voltage taps for quench localization, as all MQXFA series magnets. Therefore, quench localization is provided only by the quench antenna installed in the warm bore during magnet training.

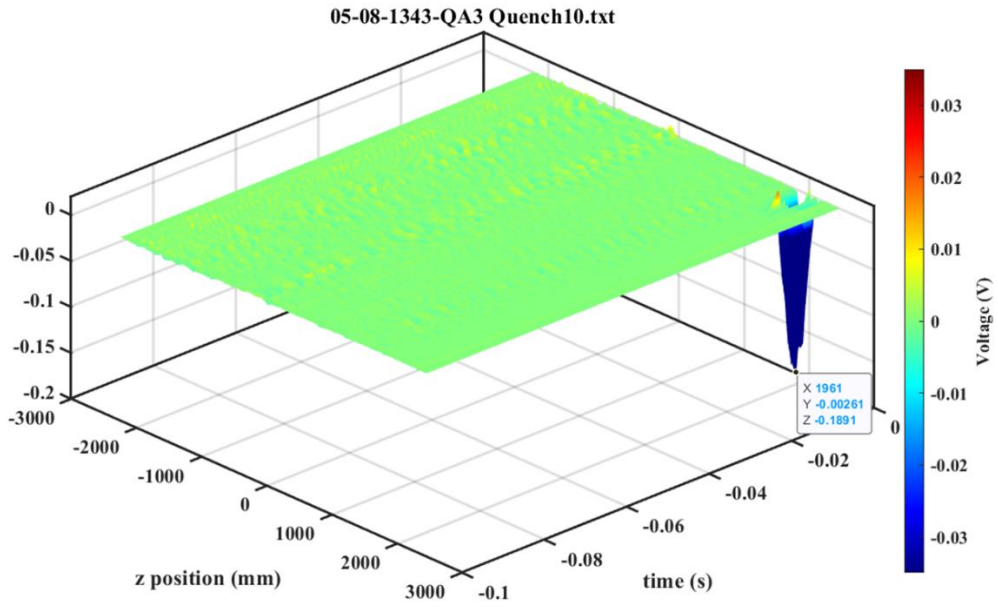

Figure 2.2: Quench antenna signal before detection of quench #10. The typical quench antenna signal strength ranges between +/- 30 mV (shown by the color bar on the right). The signal during quench #10 reached 189 mV.

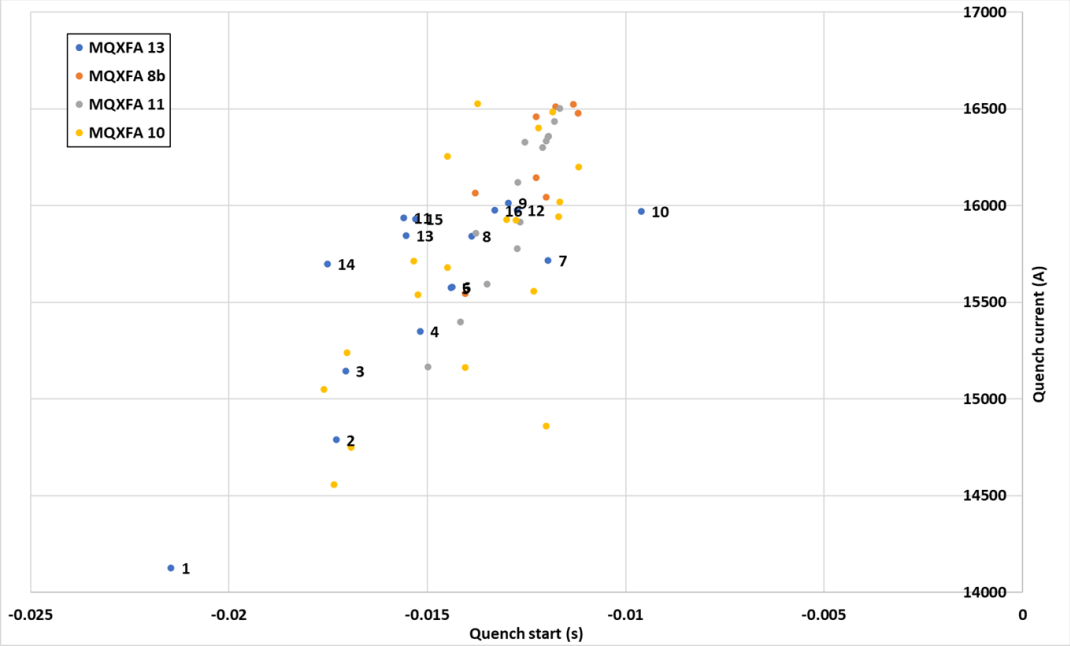

Figure 2.3: Time from quench start up to detection time (t=0) in four MQXFA magnets. Quench #10 of MQXFA13 had shorter time to detection than all other quenches even those at higher current.

2.2. Quench antenna data

A quench antenna with full length Z-coverage was used during the magnet test. It is made of 111 50 mm-long flex circuits. Theta detection was achieved using 12 full length Dipole and quadrupole buck radial circuits. In Fig. 2.4, all quench positions along Z-axis observed during the magnet training are displayed. A large number of quenches in coil 227 (Q1) took place in the same longitudinal position along the coil, at ~2000 mm from magnet. This location corresponds to the beginning of the lead end of the coil, and is consistent (within the quench antenna error of +/- 50 mm) with the location of the damaged areas found in the limiting coils of MQXFA07 [4] and MQXFA08 [5].

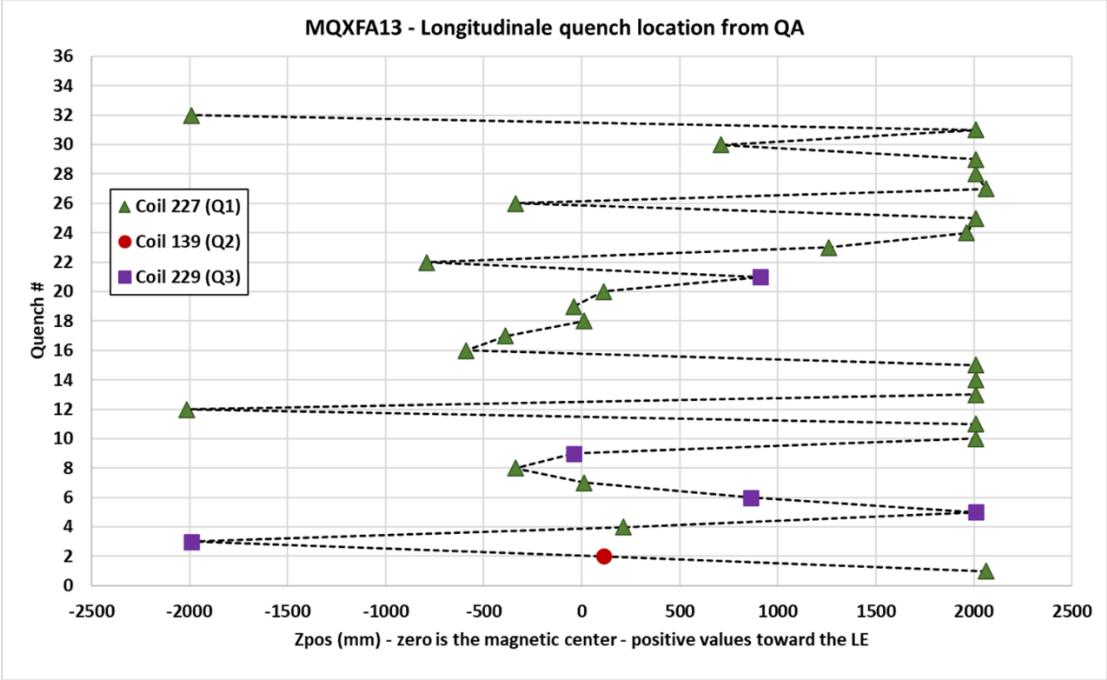

Figure 2.4: Summary of quench localization based on quench antenna along the coil axis.

2.3. Strain Gauge data analysis

The four coils of MQXFA13 were instrumented with HBM 350 Ω strain gauges, in half-bridge configuration with temperature compensation, azimuthally and axially-oriented. They are located at the return end of the magnet. In addition, coils Q1 and Q2 were instrumented with optical fibers with six FBG sensors, glued on three locations along the coils (two sensors per location: one azimuthally-oriented and one axially-oriented, at 700, 1900 and 3800 mm, from the lead end of the magnet).

Rods and shells were also instrumented with HBM 350 Ω strain gauges, the rods in full-bridge configuration, located at the return end, and the shells in half-bridge configuration, located on shells 2, 4 and 7, on the four quadrants of each of these shells.

According to the strain gauge measurements taken during magnet fabrication, coils, shells and rods were pre-loaded consistently to the target values (see figures 2.5 and 2.6), and the coil peak stress during bladder operation was maintained within the -110 MPa set as a limit in the magnet pre-load specifications. Coil Q4 was the least azimuthally-compressed coil.

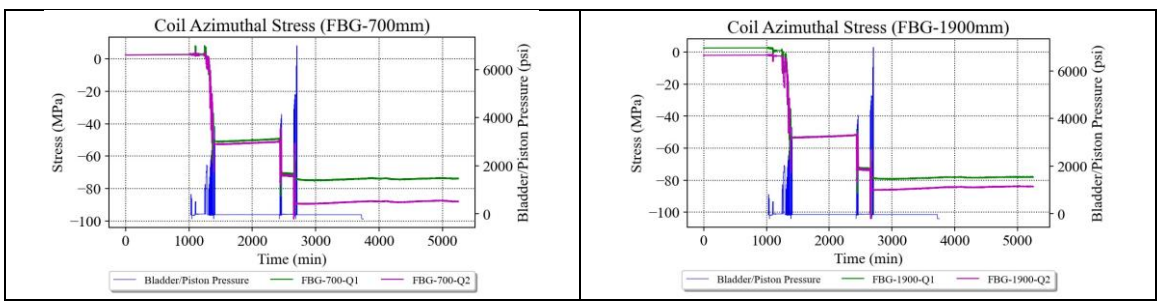

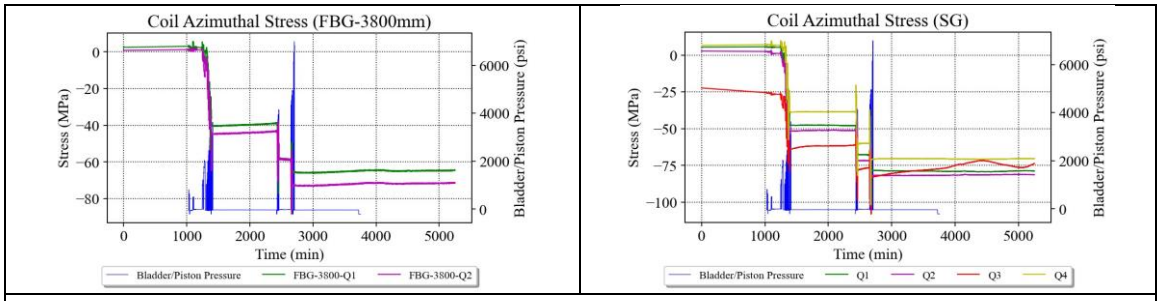

Figure 2.5: Coil azimuthal stress during bladder operation for the three optical sensor locations and the electrical strain gauge location.

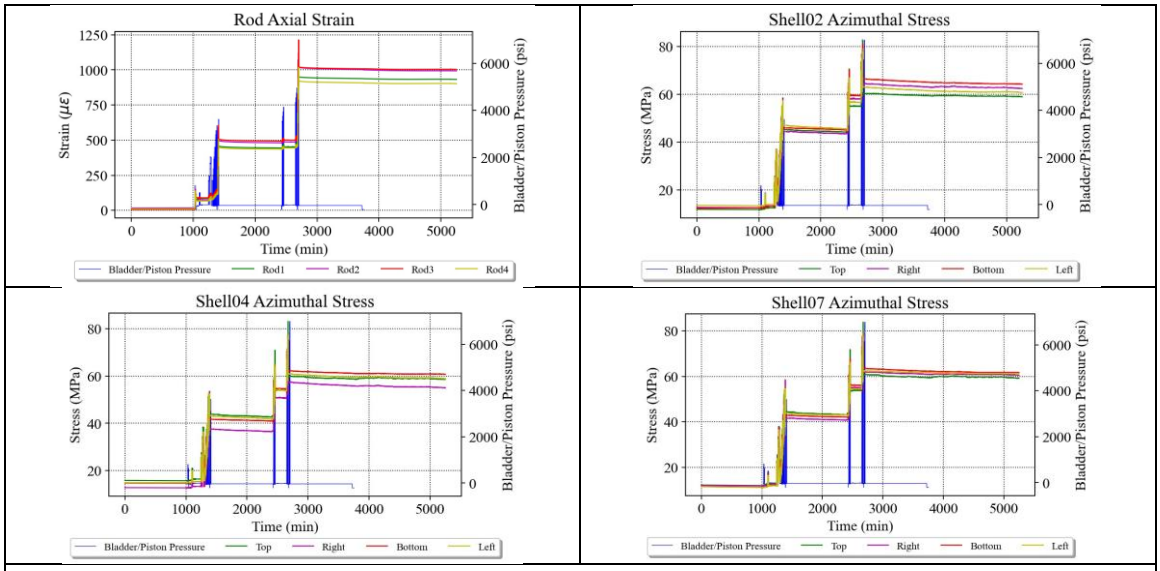

Figure 2.6: Rod axial strain and shell azimuthal stress.

Coil stain gauges were disconnected before the vertical test. Therefore, there is no coil data during the test. However, rods and shells experienced a very consistent behavior with uniform delta-stresses during powering (see figures 2.7).

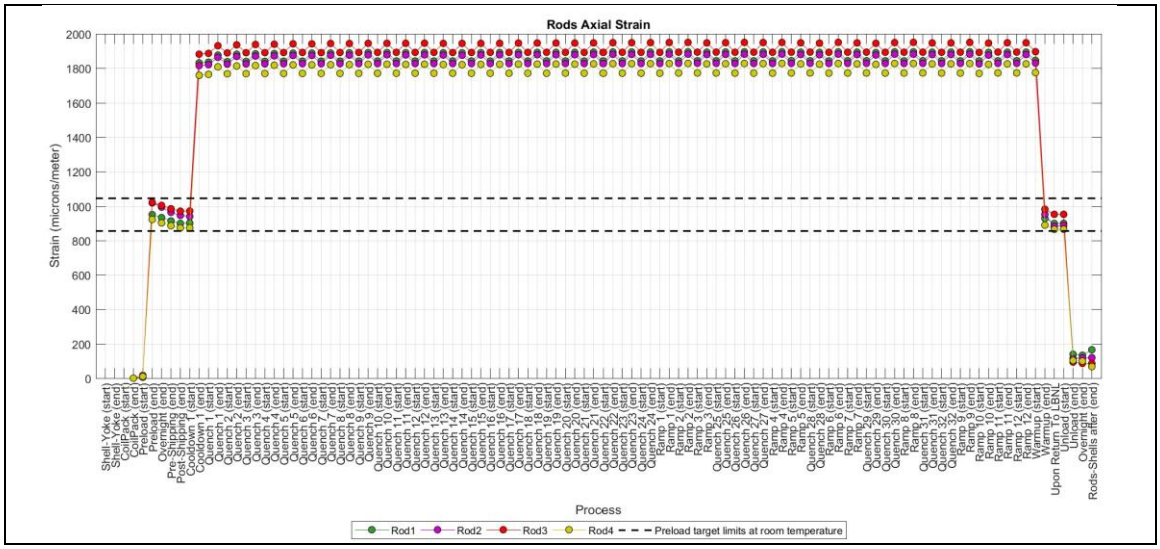

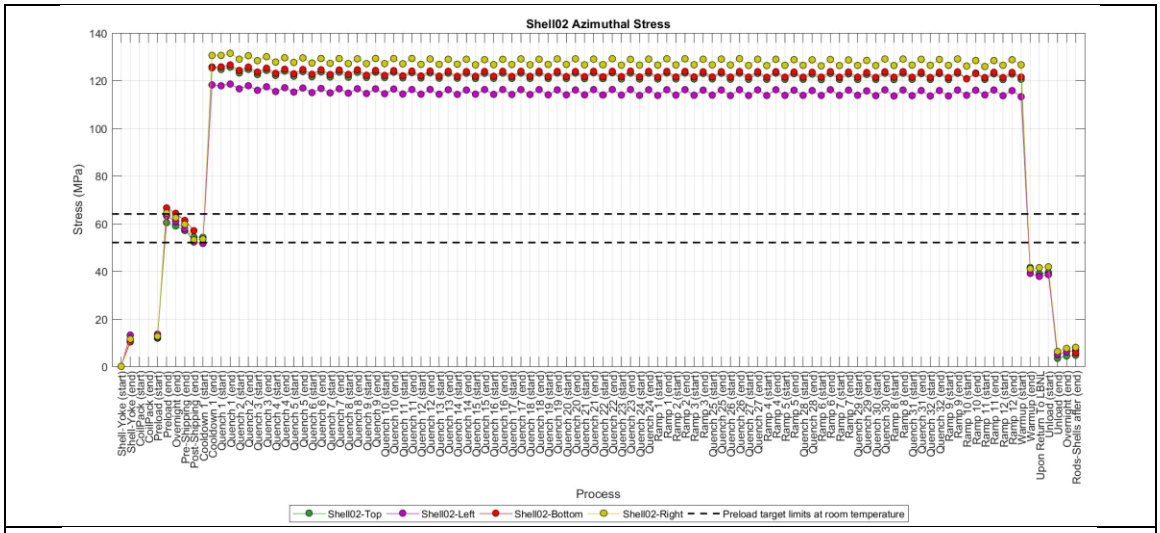
Shell02 Azimuthal Stress
Stress (MPa)
Process
Shell02-Top
Shell02-Left
Shell02-Bottom
Shell02-Right
Preload target limits at room temperature

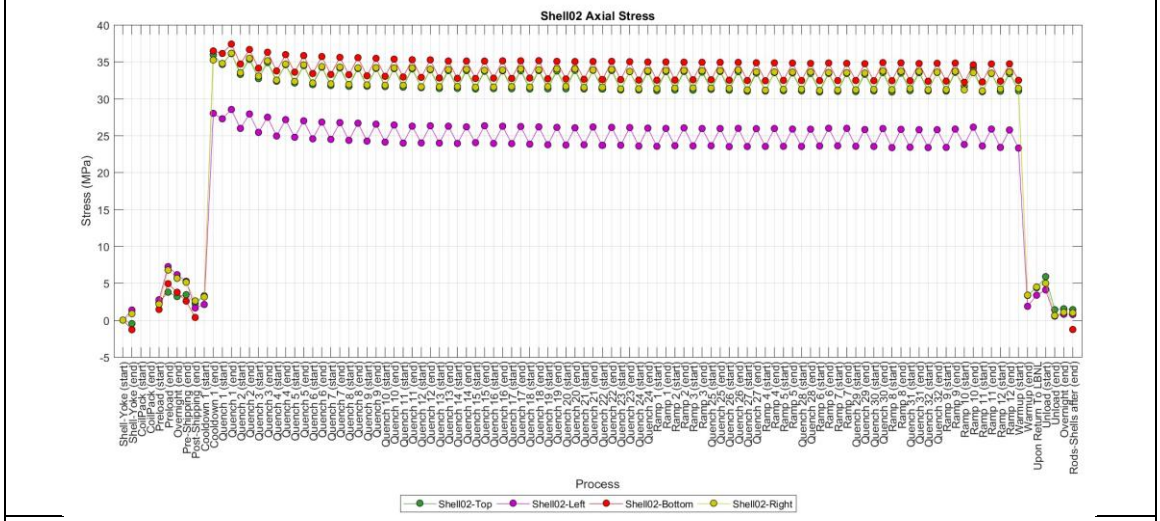
Shell02 Axial Stress
Stress (MPa)
Process
Shell02-Top
Shell02-Left
Shell02-Bottom
Shell02-Right

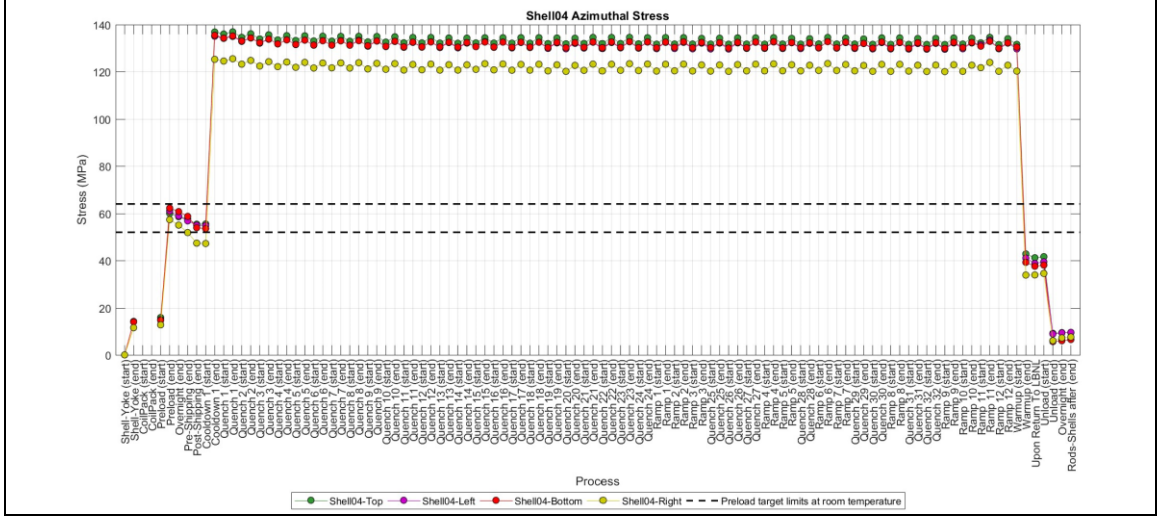
Shell04 Azimuthal Stress
Stress (MPa)
Process
Shell04-Top
Shell04-Left
Shell04-Bottom
Shell04-Right
Preload target limits at room temperature

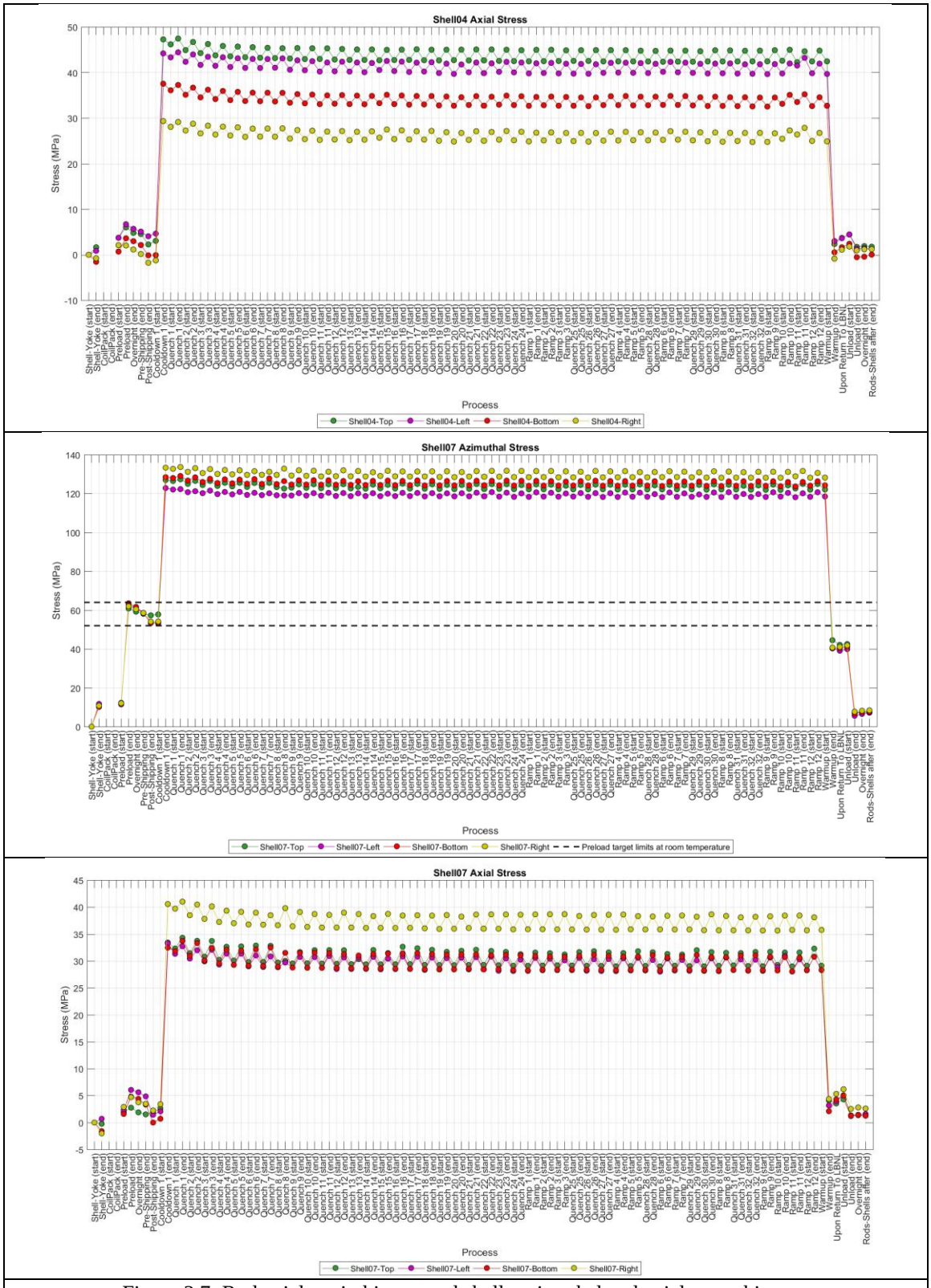

Figure 2.7: Rod axial strain history and shells azimuthal and axial stress history.

From the strain gauge data, there are no signs of abnormal behavior on coil Q1 by only looking at the rods and shell behavior. Since we do not have coil data during the test, in this case it was not possible to identify the potential mechanical causes of repeated quenches in coil Q1.

2.4. Possible limitation mechanism

The large signals during quench #10, the issues during the following training, and the location of most quenches suggested the possibility of broken Nb_3Sn filaments at or close to wedge-spacer interface in the lead end of coil 227. This is the area were broken filaments were found during the investigation of coils 214 and 213 that limited MQXFA07 and MQXFA08 [4-5]. Therefore, the subsequent investigation focused in this area.

3. Coil fabrication and magnet assembly

3.1. Coil 227 Fabrication

Coil 227 is an MQXFA coil fabricated at BNL. The main features and non-conformities of this coil and its conductor are presented in the MQXFA13 Fabrication Report [1] and are available online at [6]. Non-conformities were minor and do not appear to be connected to the limitation mechanism.

Analysis of CMM data showed that coil 227 was among the coils with the smallest arc length in the ends ever tested, together with the other coils in MQXFA13. Figure 3.1 Shows the arc length excess (difference between coil OD arc length and the nominal value) in several locations (average, maximum and minimum in the straight section, plus maximum and minimum in the ends). This observation triggered the FE analysis shown in the following chapter.

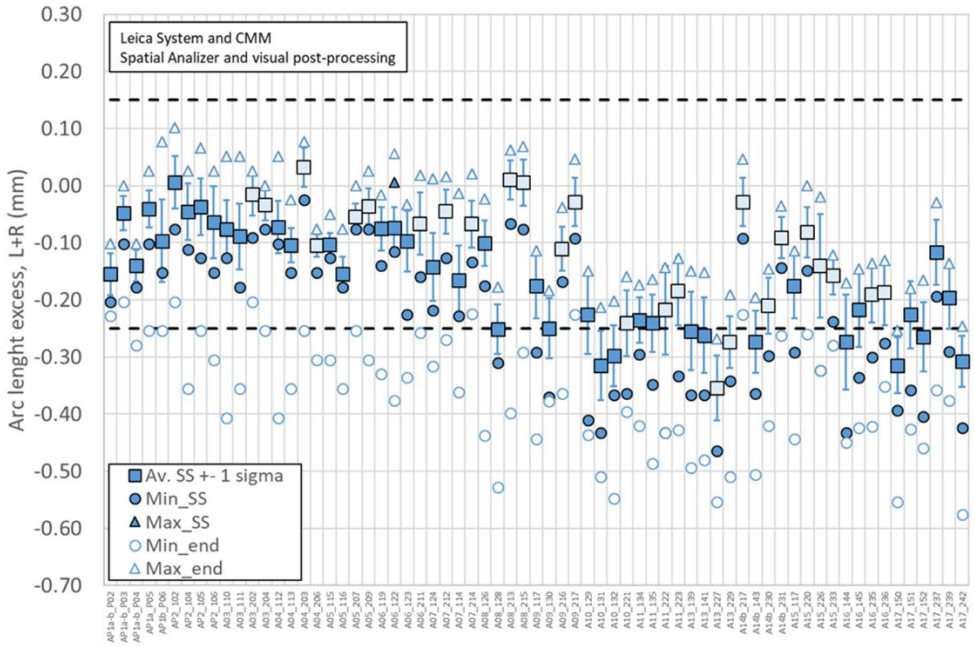

Figure 3.1 Coil arc length excess (difference between coil OD arc length and the nominal value) in several locations: average, maximum and minimum in the straight section (full markers), maximum and minimum in the ends (empty markers).

3.2. Magnet assembly, preload and NCRs

MQXFA13 assembly is described in MQXFA13 fabrication report [1]. All the non-conformities and deviations for the Magnet Structure appear to be either not critical or not relevant to coil 227 issue.

4. Magnet dis-assembly and inspection

After the test at BNL and the shipment to LBNL, MQXFA13 was inspected and disassembled at LBNL. No significant anomalies were observed during inspection and dis-assembly.

MQXFA13 structure was used for MQXFA16 assembly. Three coils (139, 141 and 229) were stored for use in MQXFA13b. Coil 227 was shipped to FNAL where post-test CMM measurements were performed, the lead end was cut and shipped to CERN for autopsy.

5. FE Analysis of MQXFA13 as-built

The effect of arc length variations over the stresses and strain experienced by the coils was studied in an octant FE model of the short model magnet MQXFS. The model assumes all coil components bonded, allowing for separation only between the wedge and the end-spacer, and the coil and the winding pole. The measured dimensional variations were introduced in the form of a contact offset between the coil elements and the radial shim package (Figure 5.1, left). A table input was used to introduce the coil pack shape variation as a function of the longitudinal position. Because of the shorter length of the FE model, the geometry deviation was limited to the portion of measurements closer to the magnet lead end (Figure 5.1, right).

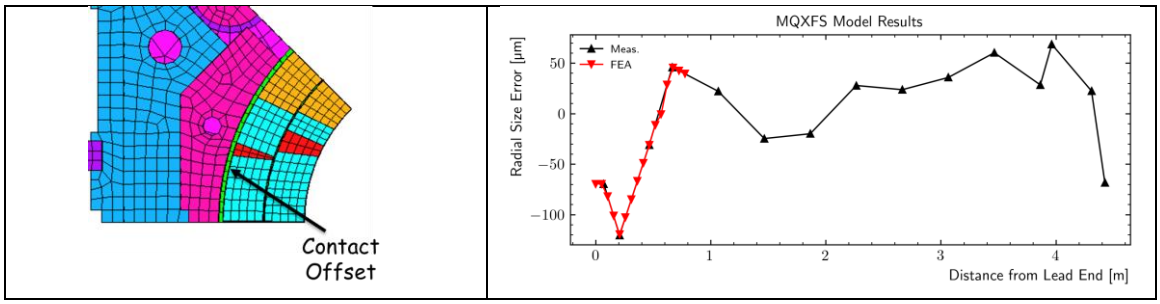

Figure 5.1: Left: Location of the contact offset used to introduce the local radial size error in the FE model. Right: Comparison between the measured radial size deviation and the FE contact offset input for the analysis.

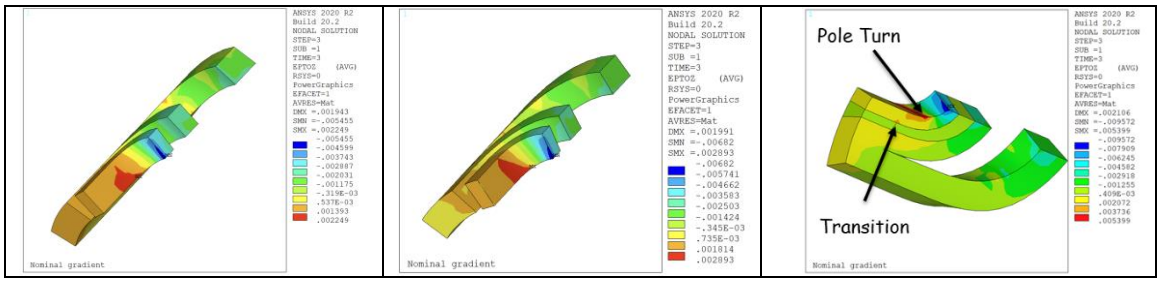

Figure 5.2: Longitudinal strain in the coil end region, considering nominal prestress and perfect initial contact conditions between the coil and the collars (left); introducing the radial size deviation measured on MQXFA13 coils (center); and lowering the room-temperature prestress to 50 MPa (right).

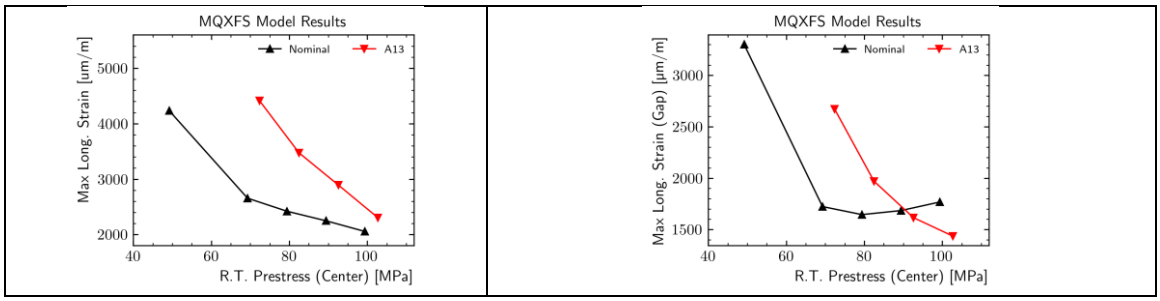

Figure 5.3: Peak longitudinal strain as a function of the applied room temperature prestress on the pole turn (left) and on the wedge/end-spacer transition (right) when considering nominal and measured (A13) coil geometries.

The model results reported in Figure 5.2 show an increase of the longitudinal strain in the end region due to the MQXFA13 coil geometry: with nominal contact conditions, the peak longitudinal strain is equal to 2249 um/m. When introducing the measured radial size deviation, this becomes equal to 2893 um/m. The effect is worsened when the azimuthal prestress is reduced: considering a room temperature pole stress of 50 MPa in the magnet center, the peak strain becomes equal to 5399 um/m. All the models show partial separation arising between the end-spacer and the wedge. Two critical regions were identified in the coil: the pole turn, and the last pole-block turn in the proximity of the wedge/end-spacer transition. While the numerical peak strain is always located on the former, it is reasonable to expect further intensification of the transition strain due to the sudden local support variation introduced by the wedge/spacer separation. This effect cannot be correctly quantified in this global magnet model because of the relatively large dimension of the coil elements.

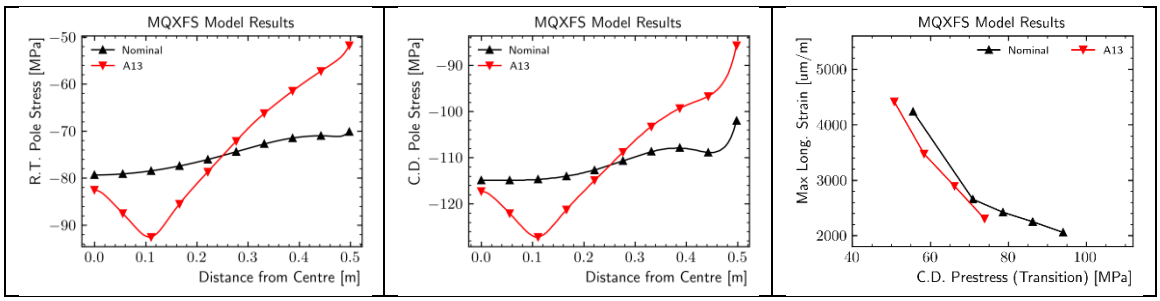

Figure 5.4: Left and center: prestress variation along the magnet length at room temperature (left), and after cooldown (center). Right: maximum longitudinal coil strain as a function of the pole prestress in the transition region after cooldown.

The variation of the strain in the two critical regions as a function of the applied prestress is provided in Figure 5.3. The results suggest that prestress reductions result in an increase of strain, and that a critical level (knee) exists where small variations of prestress result in large strain increases. The critical prestress level is increased by the reduced size of MQXFA13 coil ends.

The longitudinal strain level in the transition region is governed by the azimuthal prestress applied in that region. Figure 5.4 shows the computed stress along the winding pole for the nominal and MQXFA13 coil geometries. The smaller ends result in a prestress reduction of more than 20 MPa at cold. This prestress reduction seems to be the only significant parameter in driving the peak strain: the relationship between pole stress after cooldown at the transition longitudinal location and the peak longitudinal strain is not a function of the coil geometry (see Figure 5.4, right). As a consequence, no differences are expected between the reported results and those that would be computed on a full-length model of the magnet.

In conclusion, this FE study shows how variations of coil size along the magnet length can affect the azimuthal prestress. When the coil ends are smaller than the average, this results in an increase of the peak longitudinal strain that might lead to conductor damage.

6. Coil 227 Inspection and Autopsy

Coil 227 was inspected at LBNL after MQXFA13 disassembly. The Lead end was cut according to the plan [7] used for coil 214, which limited MQXFA7, and was sent to FNAL for further visual inspection. Subsequently, the lead end was sent to CERN for metallographic analysis.

6.1. Coil 227 Visual Inspection

The visual inspection of coil 227 lead end resulted in the following observations on the inner layer (Fig 6.1):

- There is a large bubble (delamination of the insulation on coil inner surface) at coil tip starting after the second end spacer. This bubble is typical in MQXFA coils after test.
- Four small bubbles/delaminations are visible in the pole block close to the pole tip. They may be signs of quenches in that area.
- There is a small bubble/delamination at each transition between wedge and end-spacer. This is the area where broken filaments were found in coils 213 and 214 [4-5].

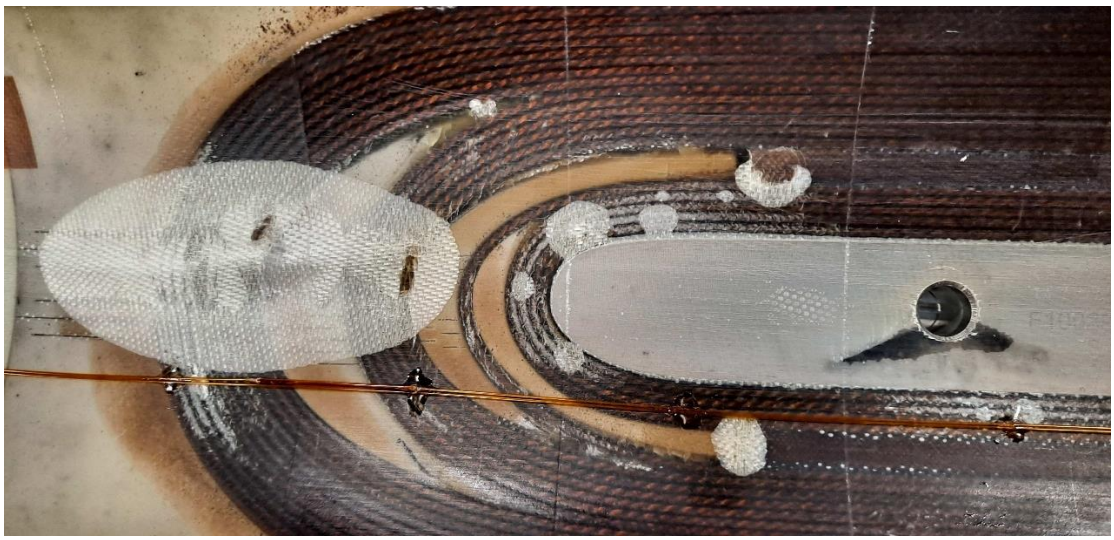

Figure 6.1: Inner surface of coil 227 in the LE region after test.

6.2. Metallographic inspection of Coil 227 Lead End

The metallographic inspection of coil 227 lead end was performed at CERN using methods and tools described in [8]. The volumes of interest for the inspection of coil 227 lead end are shown in Fig 6.2. The section extracted from the lead end is shown in Fig 6.3. The investigation started by looking at the cables facing the transitions between wedge and end-spacer. These samples are shown in Fig. 6.4.

All results of the metallographic inspection are reported in [9].

The main observations are:

- 180 filament cracks (Fig 6.5 top) were found on the cable facing the wedge-spacer transition in the pole block on the layer jump (LJ) side.
- 210 filament cracks (Fig 6.6) were found on the cable facing the wedge-spacer transition in the pole block on the opposite side to the layer jump (OLJ).
- No filament cracks were found on both cables (LJ and OLJ) facing the wedge-spacer transition in the midplane block.
- All filament cracks are located in the short segments between the wedge and the end spacer as shown in Fig 6.5 bottom.
- Cracks in the glass-filled epoxy were found between wedge and spacer in the Layer Jump side, and the epoxy separated from the wedge after cutting showing poor adhesion (Fig 6.7). Fewer cracks were found in the glass-filled epoxy in the Opposite to Layer Jump side.
- Resin filled are between wedge and spacer is larger than in the previously analyzed coils. It is 3.6 mm in the LJ side and 2.8 mm in the OLJ side, whereas it was 1.5 mm (LJ) and 2 mm (OLJ) in coil 214.

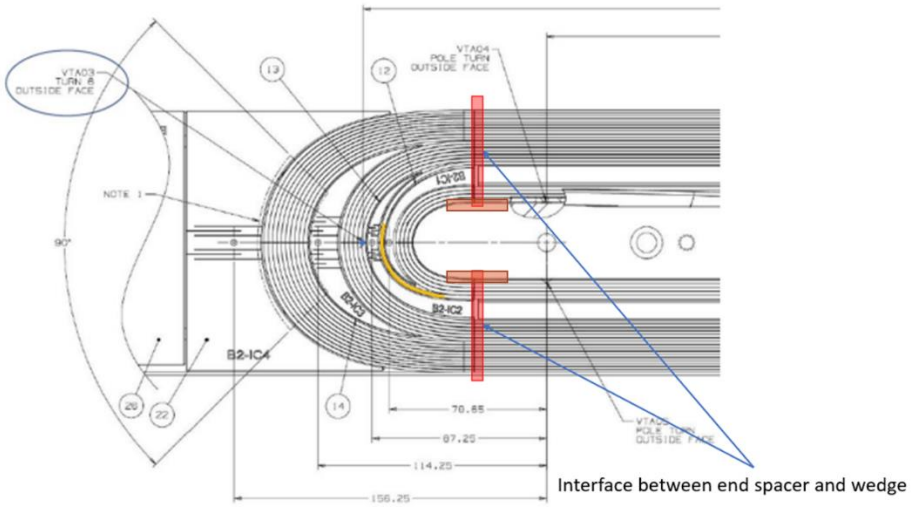

Figure 6.2. Volumes of interest (highlighted by the red boxes) for the metallurgical inspection of coil 227 lead end.

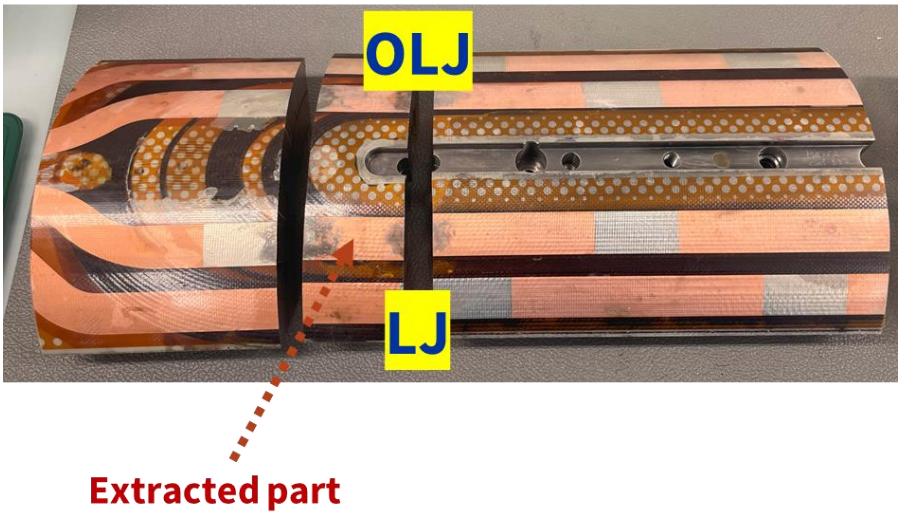

Figure 6.3. 43 mm thick slice including the transition between end spacer and wedge (in inner layer).

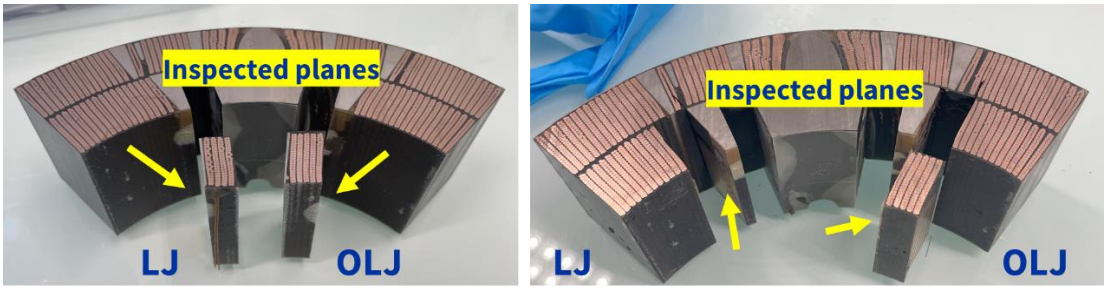

Figure 6.4. Samples extracted for looking at the cables facing the wedge-end transition.

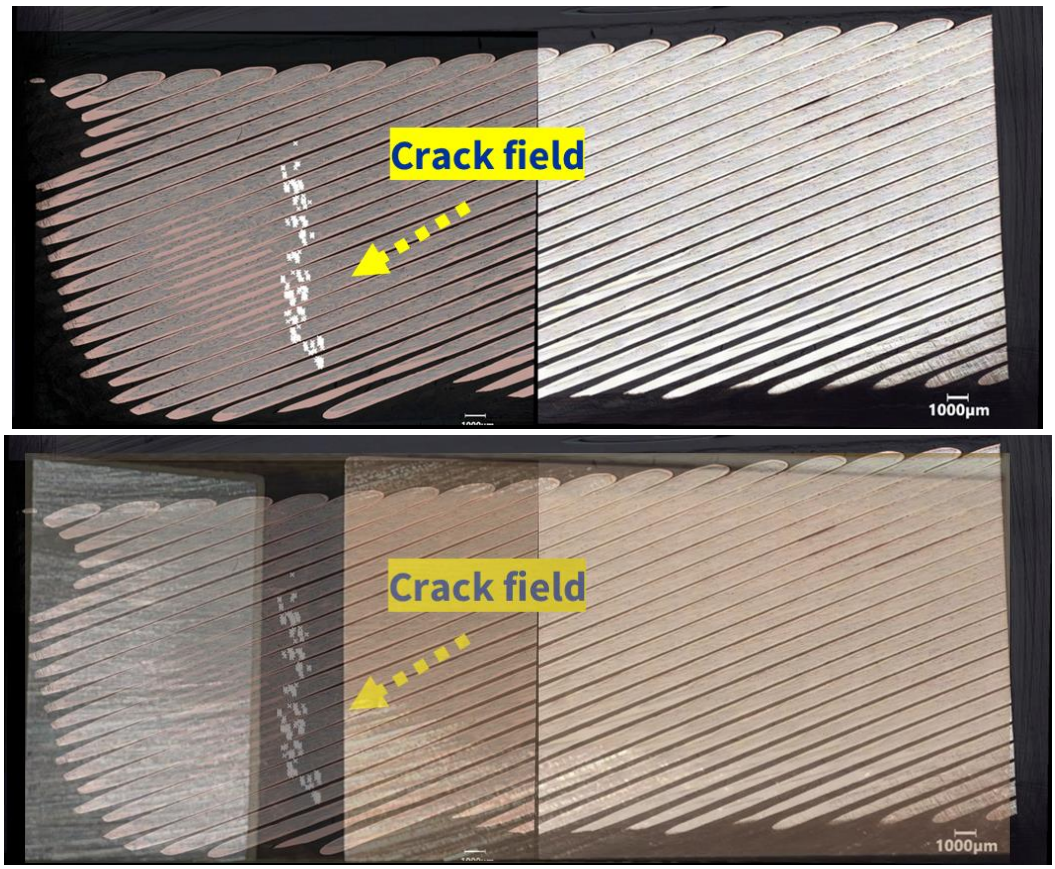

Figure 6.5. Top: Locations of broken filaments in the cable facing the wedge-spacer transition in the pole block on the layer jump (LJ) side. Bottom: A semi-transparent picture of wedge (right) and end-spacer (left) has been overlapped to the top picture in order to show the position of the crack field with respect to wedge and end-spacer.

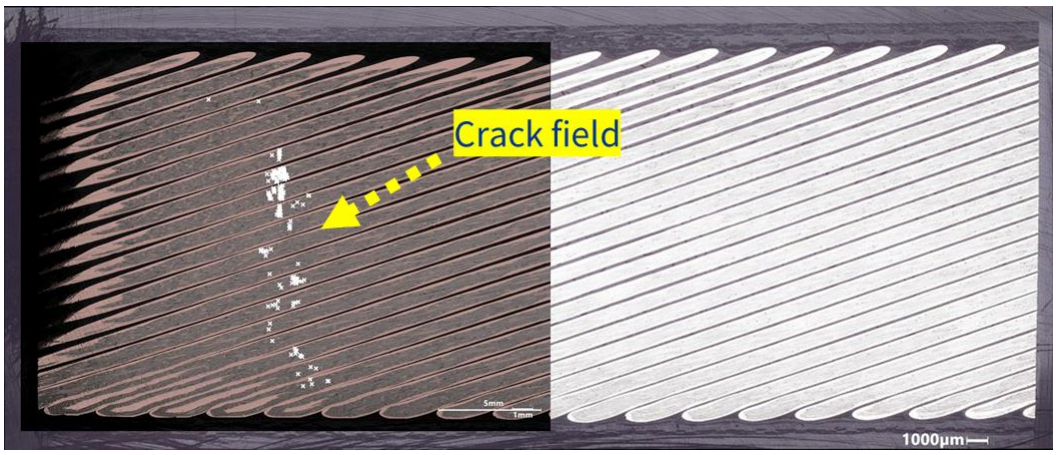

Figure 6.6. Locations of broken filaments in the cable facing the wedge-spacer transition in the pole block on the side opposite to the layer jump (OLJ).

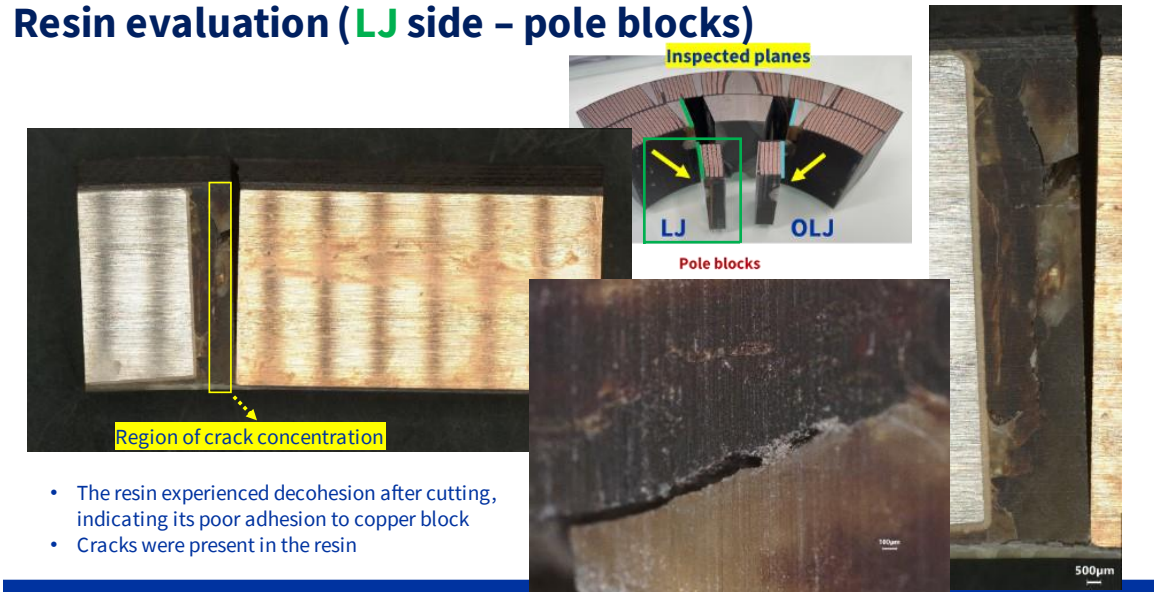

Figure 6.7 Cracks in the glass-filled epoxy between wedge and spacer in the Layer Jump side

7. Conclusions

The data and analyses presented in this report have shown that:

- Quench #10 (at 15969 A) in coil 227 had signals significantly larger than usual, suggestive of a big event, and triggered some detraining quenches in coil 227.
- Although MQXFA13 was able to hold acceptance current several times, it quenched 3 times at the first ramp-up after a ramp-down at 100 A/s. All these quenches were in coil 227.
- Analysis of CMM data showed that MQXFA13 coils had *delta arc-length* in the ends (difference between average arc-length in the straight section and in the ends) smaller than past magnets; and coil 227 was among the worst coils.
- Finite element analysis of MQXFA13 as built (simulating the average arc-length of the 4 coils in the lead ends and in the first part of the straight section) showed that a large *delta arc-length* in the ends and low pre-stress may results in tension at the wedge-spacer transition in coil ends during magnet powering.
- Metallographic inspection of the cables in coil 227 adjacent to the wedge-spacer (W-S) transitions in the inner layer of the lead end showed some cracked Nb_3Sn filaments. Cracks were found in the cables of the pole block, and no cracks were found in the cables of the midplane block. All filament cracks were at the wedge-spacer (W-S) transitions where some cracks in the epoxy were also visible.

Based on these and other findings presented in this report, we understand that the large *delta arc-length* in the ends of coil 227 together with the low prestress caused high longitudinal tension at the wedge-spacer interface during magnet powering. A crack in the epoxy or detachment from the wedge caused quench #10, and the magnet found a new equilibrium at the end of the detraining quenches #11-15. After that the magnet was able to train up to acceptance current. Nonetheless, some Nb_3Sn filaments had been broken during the event that caused quench #10 and/or the following quenches in that area (wedge-spacer transition in the lead end). These broken filaments, together with the strand magnetization due to the ramp down at -100 A/s, caused the quenches in the three ramps (#30, #33 and #36) up following the ramps down at -100 A/s.

8. References

1. MQXFA13 Fabrication report, US-HiLumi-doc-4904.
2. MQXFA13, MQXFA8b and MQXFA14b Test Results Meeting, Oct. 12, 2023, https://indico.fnal.gov/event/61415/
3. Acceptance Criteria Part A: MQXFA Magnet, US-HiLumi-doc-1103 and CERN EDMS# 2031083
4. Analysis of MQXFA07 Test Non-Conformity, US-HiLumi-doc-4293.
5. Analysis of MQXFA08 Test Non-Conformity, US-HiLumi-doc-4776.
6. MQXFA13 Coils Acceptance Review, https://indico.fnal.gov/event/56491/
7. MQXFA07 Inspection Plan, US-HiLumi-doc-4222.
8. A. Moros, et al., “A Metallurgical Inspection Method to Assess the Damage in Performance-Limiting Nb_3Sn Accelerator Magnet Coils”, IEEE Trans. Appl. Supercond., vol. 33, no. 5, Aug. 2023, Art no. 4000208.
9. Aleksandra Bartkowska, Mickael Crouvizier, Stefano Sgobba, “Metallographic inspection of MQXFA13 227 coil” CERN EDMS 3025133.